Transcription Factor Runx1 Activates Opn to Promote Tumor Progression in Head and Neck Cancer

Kai Liu
Southeast University
Huiying Hu
Southeast University
Huanyu Jiang
Southeast University
Haidong Zhang
The Affiliated BenQ Hospital of Nanjing Medical University
Shanchun Gong
The Affiliated BenQ Hospital of Nanjing Medical University
zhenkun yu (yuzhenkun@yahoo.com)
southeast university

Research

Keywords: HNSCC, RUNX1, OPN, MAPK, metastatic progression

Posted Date: June 12th, 2020

DOI: https://doi.org/10.21203/rs.3.rs-34679/v1

Abstract

Background: Metastatic progression remains a major burden for head and neck squamous cell carcinoma (HNSCC). Runt-related transcription factor 1 (RUNX1)has been reported to be associated with an aggressive phenotype in several cancers. However, the precise roles of RUNX1 underlying the metastaticprogression of HNSCC remain largely unknown.

Methods:RUNX1 expression levels in HNSCC cells and tissues were detected by quantitative real-time PCR (qPCR), Western blottingand immunohistochemistry (IHC). In vitro and in vivo assays were performed to investigate the function of RUNX1 in the metastatic phenotype and the tumorigenic capability of HNSCC cells. Luciferase reporter and chromatin immunoprecipitation (ChIP)-qPCR assays were performed to determine the underlying mechanism of RUNX1-mediated HNSCC aggressiveness.

Results:RUNX1 was increased with disease progression in patients withHNSCC.Furthermore, we found that silencing ofRUNX1 significantly decelerated the malignant progression of HNSCC cells and reduced Osteopontin (OPN) expression in vitro, and weakened the tumorigenicityof HNSCC cells in vivo. Mechanistically, we demonstrated that RUNX1 played an important role in activating MAPK signaling by directly binding to the promoter of OPN.

Conclusions: Our results provide new insight into the mechanisms underlying the facilitate metastasisability of RUNX1and reveal the therapeutic potential of targeting RUNX1 in HNSCC.

Background

Metastatic progression remains a major burden for head and neck squamous cell carcinoma (HNSCC) and is associated with eventual resistance to prevailing therapies[1]. Significantly, complex molecular transcriptional programs and downstream signaling pathways have been implicated in the development of HNSCC from premalignancy and progression to invasion, metastasis, and treatment resistance[2]. Runt-related transcription factor 1 (RUNX1), also known as acute myeloid leukemia 1 protein (AML1), is a member of RUNX family of transcription factors (RUNX1, RUNX2 and RUNX3), and is an essential master transcription factor implicated in basic cellular and developmental processes, stem cell biology and tumorigenesis[3, 4]. According to previous studies, RUNX1 plays a pivotal role in definitive hematopoiesis, is one of the most frequently mutated genes in a variety of haematological malignancies[5]. Furthermore, gene expression profiles of metastatic adenocarcinomas (lung, breast, prostate, colorectal, uterus and ovary cancers) revealed that RUNX1 is a gene whose expression pattern predicts metastasis[6]. In particular, RUNX1 was found overexpressed in oral SCC, and was essential for the growth and survival[7]. Although much is known about the roles of RUNX1 in different cancers, the mechanisms in the regulation of genes that are intimately associated with tumor progression, invasion and metastasis should be of greater concern. These genes include osteopontin, bone sialoprotein and matrix metalloproteinase 13, all of which have been implicated in metastasis[8, 9].

Osteopontin (OPN), also called secreted phosphoprotein 1 (SPP1), is a multifunctional secreted acidic glycoprotein encoded by the SPP1 gene[10]. Substantial evidence associates OPN expression with tumor invasion and metastasis in a number of cancers such as oral, breast, lung, brain, and other cancers[11–14]. Transcriptional regulation of OPN is complex and involves multiple signal transductions[15]. Identifying transcription factor that contribute to the modulation of OPN expression is of interest for therapy that aims to control the OPN-mediated metastatic phenotype. Several known cis-acting transcription factors have been identified, such as Myc, AP-1, Oct-1, Wnt/β-catenin/APC/GSK-3b/Tcf-4, Ras/RRF, TF53[16]. In addition, a previous study showed that RUNX1 has played a key role in the upregulation of the OPN gene in metastatic tumor cells, such as lung, melanoma, leukemia, colon, breast cancer cell lines[17]. However, it is not yet known whether a similar transcriptional regulation occurs between RUNX1 and OPN in HNSCC.

In this study, we set out to elucidate the function of RUNX1 in HNSCC and the role of RUNX1 in transcription regulation of OPN. The results confirmed the clinical relevance of RUNX1 and OPN in HNSCC. Our nude mice xenograft models verified that RUNX1 expression increases concomitant with disease progression. Moreover, in vitro studies established that RUNX1 is associated with higher migration and invasion ability. Significantly, we found RUNX1 has the binding ability in the OPN regulatory sequence, and OPN is known to influence the malignant phenotype of tumor cells. Thus, this evidence suggested that, in HNSCC, RUNX1 play an important role in the migration and invasion of tumor cells to control their migratory properties. Its active role in activating the OPN gene in tumor cells may help these cells to show metastatic phenotypes.

Materials And Methods

Patient samples and Cell lines

This study was approved by the Ethics Committee of BenQ Medical Center, the Affiliated BenQ Hospital of Nanjing Medical University (Nanjing, China), and patients consented to the use of the tissue specimens for research purposes. HNSCC tissues that were surgically resected were obtained from the department of pathology, BenQ Medical Center. The specimens were classified according to the 2018 NCCN criteria and TMN staging system. Histologic classification and tumor stage were reviewed by two pathologists. The HNSCC cell lines FaDu and SCC-9 were purchased from Guangzhou Cellcook Biotech Co., Ltd (Guangzhou, China). The cells were authenticated by STR profiling. FaDu cells were maintained in RPMI-1640 (Gibco, USA) medium with 10% fetal bovine serum (FBS, Gibco, USA) and 1% Penicillin/Streptomycin (Gibco, USA), SCC-9 cells were maintained in Dulbecco's modified Eagle's medium (DMEM/F12, Gibco, USA) with 10% FBS and 1% Penicillin/Streptomycin, supplemented with sodium pyruvate (CellCook, China) and hydrocortisone (CellCook, China). 293T cells were maintained in Dulbecco's modified Eagle's medium (DMEM/F12, Gibco, USA) with 10% FBS and 1% Penicillin/Streptomycin, All cells were cultured at 37 °C in a humidified 5% CO_2 atmosphere.

Lentiviral Transduction

The overexpression and knockdown of RUNX1 and OPN were performed using a lentiviral packaging system. Cells were grown to 60% confluency and infected with lentiviral vectors targeting RUNX1 and OPN (Shanghai Genechem Co., Ltd. Shanghai, China), or with negative control vectors in the presence of 10 mg/mL Polybrene (hexadimethrine bromide). The supernatant was removed after 12 hours and was replaced with complete culture medium. After 72 hours of transduction, the cells were collected for further experiments.

Cell Proliferation Assay

A Cell Counting Kit-8 (CCK-8) (Dojindo, Japan) was used to determine cell viability. 1×10^3 cells were plated in 96-well plates and incubated for 12 hours. Then medium containing CCK-8 solution (10 mL CCK-8 in 100 mL medium) was added to each well at the same time every day for 3 days. The OD values were detected at absorbances of 450 nm and 630 nm. All experiments were performed in triplicate.

Colony Formation Assay

For clonogenicity analysis, 500 viable cells were seeded in 6-well plates. Culture medium was changed every two days. After 10 days of incubation, colonies were fixed with 4% paraformaldehyde and stained with giemsa (Solarbio, China). The cells were photographed and the numbers of colonies were scored.

Migration Assay

For the scratch assays, 4×10^5 cells were seeded in 6-well plates and allowed to adhere overnight until they reached 95% ~ 100% confluency. Cells were serum-starved for 8 hours prior to beginning the assay. Subsequently, a scratch was made across the cell layer using a 100 μl pipette tip, and cell migration was monitored by recording images after 24 hours. The area of the scratch was quantified using the MiToBo plug-in for ImageJ software and plotted as a percentage of total area. For the transwell migration assay, 5×10^4 cells were seeded in triplicate in migration chambers (BD Biosciences, Bedford, MA, USA) in serum-free medium. Cells were allowed to migrate through 8 μm pores toward medium containing 10% FBS for 48 hours. Non-migrating cells were removed and cells that migrated through the membrane were fixed with 4% paraformaldehyde. Fixed cells were stained with giemsa (Solarbio, China) solution and photographed. The number of cells on the membrane was determined by counting under a microscope.

Invasion Assay

For the invasion assay, 5×10^4 cells were seeded in triplicate in Matrigel invasion chambers (BD Biosciences, San Jose, CA, USA) in serum-free medium. Cells were allowed to invade through the Matrigel and 8 μm pores toward medium containing 10% FBS for 48 hours. Non-invading cells were removed using a cotton swab and cells that invaded through the membrane were fixed with 4% paraformaldehyde. The procedure for transwell migration described above was then followed to complete the experiments.

Immunohistochemistry

Both the human tissue and mouse tissue are the same immunohistochemical procedure. Following deparaffinization and rehydration, antigen retrieval was performed using DAKO Target Retrieval Solution (DAKO, Carpinteria, CA, USA), pH6.0 in 50% glycerol at 95 °C for 20 minutes. Sections were blocked for endogenous peroxidase using hydrogen peroxide in methanol followed by treatment with 1% bovine serum albumin, 10% normal goat serum and 0.1% Triton X-100. The tissue was incubated overnight at room temperature with anti-RUNX1 antibody (1:500, Abcam, USA) and anti-OPN antibody (1:1000, Abcam, USA). The sections were incubated with anti-rabbit IgG biotinylated secondary antibodies. After incubation with streptavidin-HRP for 30 min at room temperature, sections were analyzed using a Zeiss AxioPlan microscope.

Quantitative Pcr

Total RNA was extracted using TRIzol reagent (Thermo Fisher Scientific, USA) and cleaned by DNase digestion (Zymo Research, USA). Subcellular fractionation of nuclear and cytoplasmic RNA was isolated separately using the Cytoplasmic & Nuclear RNA purification kit (Norgen BioTek, Canada). RNA was reverse transcribed into cDNA with the Superscript III first-strand synthesis system (Thermo Fisher Scientific, USA). Quantification of gene expression was conducted using Power SYBR green PCR Master Mix and the StepOnePlus Real-Time PCR system (Thermo Fisher Scientific, USA). The expression of each target gene was determined with β-actin as the normalization control. The results were analyzed to obtain the Ct values of the amplified products, and data were analyzed by the $2^{-\Delta\Delta Ct}$ method.

RUNX1 Forward: GTTTGTCGGTCGAAGTGGAAGA,

RUNX1 Reverse: AGGGTTAAAGGCAGTGGAGTGG;

OPN Forward: AGTTTCGCAGACCTGACATCC,

OPN Reverse: TTCCTGACTATCAATCACATCGG;

β-actin Forward: CACCCAGCACAATGAAGATCAAGAT,

β-actin Reverse: CCAGTTTTTAAATCCTGAGTCAAGC.

Western Blotting

Whole cell protein lysates were generated using RIPA buffer; nuclear and cytoplasmic protein lysates were generated using the NE-PER nuclear and cytoplasmic extraction kit (Thermo Scientific, USA). Both protein isolation reagents were supplemented with 25 μM MG132 and complete protease inhibitor cocktail (Roche Diagnostics, USA). Lysates were separated on a 10% acrylamide gel and immobilized on PVDF membranes (Millipore, USA). Blots were blocked using 5% bovine serum albumin (BSA, HyClone, China) before being incubated overnight at 4 °C with the following primary antibodies: anti-RUNX1 ((1:1000, Abcam, USA), anti-OPN (1:1000, Abcam, USA) and anti-GAPDH (1:1000, Proteintech, USA). GAPDH was used as loading controls. Secondary antibodies conjugated to HRP (Proteintech, USA) were used to detect proteins in conjunction with an enhanced chemiluminescent reagent (ECL; Millipore, USA) in a Bio-Rad Image Lab system. The bands were quantified using Imaging J analysis software.

Luciferase Reporter Assay

At 12–24 hours before transfection, 293T cells were plated at 2×10^5 cells per well in a six-well cell culture plate. A 2 μg measure of various DNA constructs and 0.3 μg of Renilla construct (Promega, USA) were mixed with 10 μl of lipo3000 (Qiagen, German). The mixture was incubated at room temperature for 20 minutes. After washing the cells with PBS, the DNA/ lipo3000 mixtures were transferred to the cells and incubated at 37 °C in a CO_2 incubator for 6 hours. The supernatant was replaced with complete culture medium. When cotransfection with constructs expressed various transcription factors, appropriate control plasmids pGL3 was also transfected into separate cultured cells as controls, and DNA was maintained in equal amounts. Subsequently, the transfected cells were washed with PBS and cultured for an additional 48 hours. At the end of 48 hours incubation, the transfected cells were lysed with reporter lysis buffer (Promega, USA). The enzymatic activity was measured for firefly and Renilla luciferase using Dual-Luciferase Reporter assay System (Promega, USA) and a luminometer. All luciferase assays were carried out in duplicates or triplicates and experiments were carried out at least twice.

Chromatin Immunoprecipitation Analysis

ChIP assays were performed using a ChIP Kit (Thermo Scientific, USA) according to the manufacturer s instructions. Briefly, 5×10^6 cells were treated with 1% formaldehyde to cross-link chromatin-associated proteins to DNA. The cell lysates were subjected to ultrasound to shear the DNA into fragments. 10% of each sample was used as input reference control. Chromatin protein suspensions were then incubated with 10 μl of anti-RUNX1 antibody (Abcam, USA) or control anti-IgG antibody (CST, USA). All the above chromatin supernatants were incubated with 20 μL magnetic protein A/G beads overnight at 4 °C with rotation. The protein-DNA complexes were reversed and purified for pure DNA, and then were submitted to SYBR green (Applied Biosystems) qPCR analysis with an ABI Prism 7900HT Fast RealTime PCR system. The following primers were used for quantitative ChIP-PCR

RUNX1 Forward: TCCCGCTGGAATTAAGAAAA,

RUNX1 Reverse: CCCACGGGAATGATTCAATA.

In Vivo Xenograft Assay

Six-week-old athymic BALB/c nude female mice were used for in vivo xenograft assay. All animal experiments were performed according to the Southeast University Animal Care Facility and National Institutes of Health guidelines. Approximately 5×10^6 FaDu cells with different treatment conditions were harvested and suspended in 150 ml of PBS and Matrigel (BD Bio-science, USA) (1:1) and injected subcutaneously into the flank of each mouse. Mice were weighed, and the tumor size was measured using bilateral caliper measurements. The size of subcutaneous tumors and weight of the mice were recorded every two days. Tumor volume (V) was calculated according to the formula $V = 0.5 \times$ Tumor maximum diameter (L) × the right angle diameter to that axis $(W)^2$. At the end of treatment, mice were sacrificed, and the tumors were removed and used for immunohistochemical staining.

Analysis of RUNX1 expression and patient survival using public data sets

RUNX1 expression and survival in HNSCC patients was analyzed using the Cancer Genome Atlas (TCGA) database (https://www.r-project.org/) and Ginos Head-Neck Statistics based on Oncomine database (http://www.oncomine.com)[18].

Statistical analysis

The SPSS 23.0 (IBM, USA) and GraphPad Prism (version 7.01, USA) statistical analysis software programs were used for statistical analysis of the experimental data. Each experiment was repeated at least three times. The differences in mean values among groups were evaluated and expressed as the mean ± SEM. A P-value less than 0.05 was considered statistically significant (*P < 0.05, **P < 0.01, ***P < 0.001, ****P < 0.0001). Student's t-test was used to analyze the expression of cell protein markers, cell viability, relative mRNA levels, migrated cells and invaded cells.

Results

RUNX1 expression is increased with disease progression in HNSCC.

To investigate the clinical relevance of RUNX1 in HNSCC progression and metastasis, we initially conducted a study to determine RUNX1 protein expression in HNSCC tissues as well as RUNX1 RNA expression in a relevant publicly available dataset. As shown in Fig. 1A, **Fig. S1A** and **Table**, in cancerous tissues where RUNX1 was present, the percentage of RUNX1 positive cells was substantially more than in the normal head-neck tissues. Notably, the percentage of RUNX1 positive cells was as the tumor pathology grade advanced.

Table
Associations between clinicopathological characteristics and scores of RUNX1 and OPN in 29 HNSCC patients.

Characteristics	RUNX1 n(%)			OPN n(%)		
	Low	High	*P* value	Low	High	*P* value
Age(y)						
≥60	8(27.6)	11(37.9)	0.234	5(17.2)	14(48.3)	0.303
<60	2(6.9)	8(27.6)		1(3.5)	9(31.0)	
Gender						
Male	9(31.0)	19(65.5)	0.161	5(17.2)	23(79.3)	0.046
Female	1(3.5)	0(0)		1(3.5)	0(0)	
Clinical stage						
□	8(27.6)	1(3.5)	<0.001	3(10.3)	6(20.7)	0.659
□	2(6.9)	2(6.9)		1(3.5)	3(10.3)	
□	0(0)	9(31.0)		1(3.5)	8(27.6)	
□	0(0)	7(24.1)		1(3.5)	6(20.7)	
T classification						
T1	8(27.6)	1(3.5)	<0.001	3(10.3)	6(20.7)	0.732
T2	2(6.9)	4(13.8)		1(3.5)	5(17.2)	
T3	0(0)	7(24.1)		1(3.5)	6(20.7)	
T4	0(0)	7(24.1)		1(3.5)	6(20.7)	
N classification						
N0	8(27.6)	10(34.5)	0.134	2(6.9)	16(55.2)	0.056
N1	2(6.9)	3(10.3)		3(10.3)	2(6.9)	
N2	0(0)	6(20.7)		1(3.5)	5(17.2)	
N3	0(0)	0(0)		0(0)	0(0)	
M classification						
M0	10(34.5)	19(65.5)		6(20.7)	23(79.3)	
M1	0(0)	0(0)		0(0)	0(0)	
Smoking						

No	3(10.3)	2(6.9)	0.187	1(3.5)	4(13.8)	0.967
Yes	7(24.1)	17(58.6)		5(17.2)	19(65.5)	
Drinking						
No	8(27.6)	14(48.3)	0.706	3(10.3)	19(65.5)	0.096
Yes	2(6.9)	5(17.2)		3(10.3)	4(13.8)	

To determine the changes in RUNX1 expression at the primary site of cancer initiation, xenograft tumor from mice injected with the FaDu cells were sacrificed at 1, 2, 4, and 8 weeks of age. These time points represent early through late stages of disease progression. RUNX1 expression in xenograft tumor increased concomitant with disease progression, and with strong nuclear expression evident at 8 weeks (Fig. 1B **and Fig. S1B**). This observation was consistent with the results of clinical tissue samples.

We therefore addressed whether there is a clinical relationship of RUNX1 expression in HNSCC patient tumors with survival using publically available datasets. We analyzed the differential protein and mRNA expression of RUNX1 between cancer samples and normal samples, and the relationship of expression levels of RUNX1 in HNSCC samples with patient survival. In this analysis (Fig. 1C **and Fig. S1C-D**), the RUNX1 protein levels were significantly upregulated in most clinical HNSCC tissues (15 normal and 29 tumor samples, $p < 0.01$) and in 3 pairs of fresh samples. As shown in Fig. 1D and **Fig. S1E**, The RUNX1 mRNA expression was significantly elevated in HNSCC samples relative to that in normal tissue samples based on TCGA dataset (31 normal and 91 tumor samples, $p < 0.05$) and oncomine dataset (13 normal and 41 tumor samples, $p < 0.0001$)[18]. The Kaplan-Meier analysis in the TCGA dataset indicated no significant correlation ($p = 0.608$) between RUNX1 expression levels and patient survival time (**Fig. S1F**).

Runx1 Loss Decelerates The Malignant Progression Of Hnscc

To study the biological function of RUNX1 in HNSCC, we established RUNX1-silenced cell lines using a lentiviral vector carrying shRNA in FaDu and SCC-9 cells, and showed a significant decrease in RUNX1 mRNA and protein expression compared to the expression levels in control cells (Fig. 2A-B **and Fig. S2A-B**).

In cell growth and metastasis, the HNSCC cells treated with shRUNX1 were analyzed. The cell proliferation rate was significantly decreased in cells with knockdown of RUNX1 compared with control (Fig. 2C-D). As shown in Fig. 2E, markedly slower wound closure was observed in cells transfected with shRUNX1 by a wound healing assay. Moreover, the results from transwell assays revealed that knockdown of RUNX1 significantly decreased the migration and invasion abilities of HNSCC cells

(Fig. 2F). Together, these data showed that knockdown expression of RUNX1 could impede HNSCC cell growth and metastasis.

To address experimentally whether RUNX1 loss decelerates HNSCC tumor growth, $FaDu^{shRUNX1}$ and $FaDu^{sh-NC}$ cells were injected subcutaneously into the flank of each mouse (Fig. 2G). The results indicated that the ability of tumor proliferation was inhibited in the shRUNX1 group compared to that of sh-NC groups, as indicated by the final xenograft tumor volume and weight (Fig. 2H). Together, these findings verified that deregulation of RUNX1 in HNSCC might reduce the disease progression by decreasing cell proliferation, migration and invasion.

The interrelationship between RUNX1 and OPN.

To search for the putative correlation between RUNX1 and OPN, we analyzed using clinical samples data, further corroborated by TCGA and oncomine databases. Firstly, we found the protein expression levels of OPN were significantly upregulated in most clinical HNSCC samples (15 normal and 29 tumor samples, $p < 0.0001$) (Fig. 3A). Similarly, the mRNA expression of OPN were significantly elevated in HNSCC samples on TCGA database (31 normal and 91 tumor samples, $p < 0.05$) and Oncomine database (13 normal and 41 tumor samples, $p < 0.0001$) (Fig. 3B **and Fig. S3A**). Next, clinical data showed a positive correlation between the expression of RUNX1 and OPN ($R = 0.38$, $P < 0.05$) (Fig. 3C), and the TCGA dataset showed a similar result ($R = 0.36$, $P < 0.001$) (Fig. 3D). In the Ginos head-neck dataset from oncomine[18], we found a significant co-expression of RUNX1 and OPN (correlation coefficient = 0.767) (**Fig. S3B**). Finally, the Kaplan-Meier analysis in the TCGA dataset indicated no significant correlation ($p = 0.6301$) between OPN expression levels and patient survival time (Fig. S1F).

Prompted by the data mining results, we next assessed the inter-regulation of RUNX1 and OPN in vitro and in vivo. In studying the subcellular localization of RUNX1 and OPN, we learned that a small portion of OPN is localized in the nucleus, and then turned our attention to the underlying mechanism by which RUNX1 and OPN regulate each other in the nucleus. Interestingly, we observed a concurrent loss of OPN mRNA and protein upon RUNX1 deletion in nucleus and cytoplasm of HNSCC cells (Fig. 3E-F and **Fig. S3D-G**). However, RUNX1 mRNA and protein levels were not affected by OPN deletion (Fig. 3G-H and **Fig. S3H-K**). Moreover, in vivo experiments also confirmed that the expression of RUNX1 did not change significantly in xenograft tumors treated with different OPN conditions (Fig. 1F). These results motivated us to study the regulation of OPN by RUNX1.

Runx1 Has Direct Roles In Transcription Regulation Of Opn

RUNX1 was predicted to bind to the OPN DNA promoter at three possible binding sites by the Jaspar database (http://jaspar.genereg.net/), which is an open-access database for eukaryotic transcription factor binding profiles (Fig. 4A and **Fig. S4A**). ChIP-qPCR experiments using anti-RUNX1 antibody revealed that only one of the putative binding sites of the RUNX1 protein to the OPN promoter in FaDu

cells showed significant binding (Fig. 4B-C), and the remaining two are not obviously bounding (**Fig. S4B-C**).

To better understand the role played by RUNX1 in the regulation of OPN, we generated a reporter construct containing the 1,000 bp region upstream of the transcriptional start site of OPN upstream of luciferase. We transfected 293T cells with RUNX1 overexpression or the respective controls together with the OPN reporter construct and analyzed luciferase expression. The results showed that the overexpression of RUNX1 significant increased OPN promoter activity (Fig. 4D). Thus, these data suggest that RUNX1 stimulates OPN expression at the transcriptional level.

RUNX1 mediates HNSCC cell metastasis and MAPK pathway activation via stimulating OPN

We further investigated whether RUNX1-mediated cancer metastasis is related to OPN, Both sh-RNA and the overexpression lentivirus vector were used to knockdown and overexpress of RUNX1 and OPN in FaDu cells. The effects of RUNX1 and OPN on HNSCC cells were investigated by adding shOPN lentiviral vector to RUNX1 overexpressed stable strain for further transfection. RUNX1-overexpress significantly increased cell proliferation, which could be attenuated by further OPN-knockdown in FaDu cells (Fig. 5A). The similar patterns were observed in wound healing and Transwell experiments. Markedly faster wound closure was observed in RUNX1-overexpress cells. Moreover, overexpression of RUNX1 significantly increased the migration and invasion abilities of FaDu cells. Next, our results showed that the migration and invasion abilities were antagonized in cells with further OPN downregulation (Fig. 5B-E).

Since it has been shown that OPN could promote tumor progression through the MAPK pathway[19, 20], we sought to examine the protein markers expression levels of the MAPK pathway, in OPN-knockdown HNSCC cells with the situation of RUNX1-overexpress. Under the overexpression of RUNX1, the expression levels of p-MEK and p-ERK were enhanced. On the contrary, with the downregulation of OPN, this expression level is significantly weakened (Fig. 5F and **Fig. S5**), suggesting that RUNX1 might activates the MAPK pathway accompanied by OPN stimulation.

Discussion

As previously demonstrated, the RUNX1 protein acts as either tumor suppressor or oncogene in different cancer types, depending on activate or repress target gene expression in different cellular context [21, 22]. Indeed, RUNX1 has displayed dual roles in breast cancer and also in gastric cancer[23–26]. The key findings of this study support the oncogenic function of RUNX1 in HNSCC. The clinical samples data were indicative for strong RUNX1 protein overexpression concomitant with higher grade in the HNSCC tissues. Complementary in vivo studies demonstrate that RUNX1 expression increases concomitant with disease progression in the xenografts of mice. Furthermore, we found that the expression of RUNX1 was increased in clinical HNSCC tissues, consistent with the results from TCGA and Oncomine database. Although the TCGA data showed no correlation between RUNX1 expression and patient survival time, in vitro experiment, RUNX1 knockdown in the HNSCC cells results in a marked abrogation of migration and invasion ability than control cells. Moreover, RUNX1 loss weakened the tumorigenesis ability in mice. Our

results are in line with a previous study in which a comprehensive analysis of RUNX1 protein in epithelial cancer was performed[7].

The above findings persuaded us to investigate the functional implication of RUNX1 in mechanisms of invasion and metastasis. Mammalian RUNX1 transcription factors mediate the homeostasis of malignant cells through their ability to promote gene activation[4]. Recent genetic studies have highlighted a potential role for OPN in HNSCC, and a high level of OPN activity has been reported to be related to metastasis and poor outcomes of HNSCC patients[27–29]. Our study examined the correlation between RUNX1 and OPN using clinical samples, TCGA and Oncomine database. The results show that RUNX1 is positively correlated with OPN expression. In parallel, our study revealed that RUNX1 dramatically affect OPN expression in HNSCC cells, and nuclear /cytoplasmic expression of RUNX1 was positively correlated with OPN expression. In contrast, RUNX1 expression was not influenced by OPN deletion, implying a pathological significance for RUNX1 regulation of OPN in HNSCC development.

As a transcription factor, RUNX1 may regulate the transcription of target genes in many ways[30]. Our luciferase reporter assay verified that RUNX1 stimulated the transcriptional activity of the OPN promoter. Moreover, this speculation is further supported by the finding that RUNX1 can bind to the OPN promoter in a ChIP-qPCR analysis. Consistent with this result, RUNX1 is a key transcription factor that can directly binds to the OPN regulatory sequence to upregulate the gene expression in metastatic tumor cells[17]. Collectively, our in vitro data strongly suggests that OPN is a RUNX1-target gene.

It is noteworthy that some research has verified that RUNX1, as a transcription factor, cooperates with its target genes to promote tumor metastasis[31]. To verify whether RUNX1-mediated cancer metastasis is related to OPN, we evaluated cancer-related phenotypic properties of the cells including proliferation, migration and invasion. RUNX1 overexpress exhibited a significantly greater ability to migrate and invade compared with the control cells. Meanwhile, knockdown OPN showed the opposite effect. Notably, when RUNX1 overexpression and OPN knockdown were simultaneously present, the phenotype is neutralized. This finding supports the idea that RUNX1 mediates HNSCC cell metastasis via directly stimulating OPN. Additionally, we found RUNX1 overexpress was associated with upregulation of typical markers from the MAPK pathway, representing one of the major oncogenic pathways implicated in HNSCC etiology[32]. Similarly, other study has shown a positive correlation between RUNX1 and the MAPK signaling pathway in cancer[33]. Furthermore, we verified that these markers also appear to be neutralizing when RUNX1 overexpression and OPN knockdown coexist.

Conclusions

In conclusion, we have shown that RUNX1 transcription factor acts as an oncogene to facilitate metastasis in HNSCC by directly stimulating OPN transcription to activate the MAPK signaling pathway. These findings enhance our understanding of HNSCC metastasis. In addition, these results of our study highlight the therapeutic potential of targeting the oncogenic activity of RUNX1 in HNSCC.

Abbreviations

HNSCC
Head and neck squamous cell carcinoma; RUNX1:Runt-related transcription factor 1; OPN:Osteopontin; SPP1:Secreted phosphoprotein 1; MAPK:Mitogen-activated protein kinase; TCGA:the Cancer Genome Atlas.

Declarations

Acknowledgements

The authors thank all patients involved in this study.

Authors' contributions

KL performed experiments, analyzed data and wrote the paper; HH, HJ, HZ and SG performed some experiments and analyzeddata; KL and ZY initiated the study, designed experiments and wrote thepaper. All authors read and approved the final manuscript.

Funding

This work was funded by Programs of Nanjing Scientific Research and Technology Development Program Funding (201803072), and Programs of Jiangsu Provincial Commission of Health and Family Planning Funding (K2019015).

Availability of data and materials

All data and materials can be provided upon request.

Ethics approval and consent to participate

This study was approved by the Ethics Committee of BenQ Medical Center,Nanjing MedicalUniversity and was conducted in accordance with the government policiesand the Declaration of Helsinki. Written informed consent was obtained fromall patients.

Consent for publication

Not applicable.

Competing interests

The authors declare that they have no competing interests.

Author details

[1]School of Medicine, Southeast University, 87 Dingjiaqiao, Hunan Road, Nanjing 210009, Jiangsu, China.[2]Department of Otolaryngology Head and Neck Surgery, BenQ Medical Center, The Affiliated BenQ Hospital of Nanjing Medical University, 71 Hexi Street, Nanjing 210019, Jiangsu, China

References

1. Moy JD, Moskovitz JM, Ferris RL: **Biological mechanisms of immune escape and implications for immunotherapy in head and neck squamous cell carcinoma**. *European journal of cancer (Oxford, England*: 1990) 2017, **76**:152–166.
2. Ferris RL, Grandis JR. NF-kappaB gene signatures and p53 mutations in head and neck squamous cell carcinoma. Clinical cancer research: an official journal of the American Association for Cancer Research. 2007;13(19):5663–4.
3. Mevel R, Draper JE, Lie ALM, Kouskoff V, Lacaud G. **RUNX transcription factors: orchestrators of development**. *Development (Cambridge, England)* 2019, 146(17).
4. Ito Y, Bae SC, Chuang LS. The RUNX family: developmental regulators in cancer. Nature reviews Cancer. 2015;15(2):81–95.
5. Liu P, Tarle SA, Hajra A, Claxton DF, Marlton P, Freedman M, Siciliano MJ, Collins FS. Fusion between transcription factor CBF beta/PEBP2 beta and a myosin heavy chain in acute myeloid leukemia. Science. 1993;261(5124):1041–4.
6. Ramaswamy S, Ross KN, Lander ES, Golub TR. A molecular signature of metastasis in primary solid tumors. Nat Genet. 2003;33(1):49–54.
7. Scheitz CJ, Lee TS, McDermitt DJ, Tumbar T. Defining a tissue stem cell-driven Runx1/Stat3 signalling axis in epithelial cancer. EMBO J. 2012;31(21):4124–39.
8. Blyth K, Cameron ER, Neil JC. The RUNX genes: gain or loss of function in cancer. Nature reviews Cancer. 2005;5(5):376–87.
9. Inman CK, Shore P. The osteoblast transcription factor Runx2 is expressed in mammary epithelial cells and mediates osteopontin expression. J Biol Chem. 2003;278(49):48684–9.
10. Castello LM, Raineri D, Salmi L, Clemente N, Vaschetto R, Quaglia M, Garzaro M, Gentilli S, Navalesi P, Cantaluppi V, et al. Osteopontin at the Crossroads of Inflammation and Tumor Progression. Mediat Inflamm. 2017;2017:4049098.
11. Qin X, Yan M, Wang X, Xu Q, Wang X, Zhu X, Shi J, Li Z, Zhang J, Chen W. Cancer-associated Fibroblast-derived IL-6 Promotes Head and Neck Cancer Progression via the Osteopontin-NF-kappa B Signaling Pathway. Theranostics. 2018;8(4):921–40.
12. Gu M, Zheng X. Osteopontin and vasculogenic mimicry formation are associated with response to neoadjuvant chemotherapy in advanced breast cancer. OncoTargets therapy. 2017;10:4121–7.
13. Lin X, Lin BW, Chen XL, Zhang BL, Xiao XJ, Shi JS, Lin JD, Chen X. PAI-1/PIAS3/Stat3/miR-34a forms a positive feedback loop to promote EMT-mediated metastasis through Stat3 signaling in Non-small cell lung cancer. Biochem Biophys Res Commun. 2017;493(4):1464–70.

14. Zhao H, Chen Q, Alam A, Cui J, Suen KC, Soo AP, Eguchi S, Gu J, Ma D. The role of osteopontin in the progression of solid organ tumour. Cell death disease. 2018;9(3):356.
15. Pang X, Gong K, Zhang X, Wu S, Cui Y, Qian BZ. Osteopontin as a multifaceted driver of bone metastasis and drug resistance. Pharmacological research. 2019;144:235–44.
16. Flajollet S, Tian TV, Flourens A, Tomavo N, Villers A, Bonnelye E, Aubert S, Leroy X, Duterque-Coquillaud M. Abnormal expression of the ERG transcription factor in prostate cancer cells activates osteopontin. Molecular cancer research: MCR. 2011;9(7):914–24.
17. Liu YN, Kang BB, Chen JH. Transcriptional regulation of human osteopontin promoter by C/EBPalpha and AML-1 in metastatic cancer cells. Oncogene. 2004;23(1):278–88.
18. Ginos MA, Page GP, Michalowicz BS, Patel KJ, Volker SE, Pambuccian SE, Ondrey FG, Adams GL, Gaffney PM. Identification of a gene expression signature associated with recurrent disease in squamous cell carcinoma of the head and neck. Cancer research. 2004;64(1):55–63.
19. Liu J, Liu Q, Wan Y, Zhao Z, Yu H, Luo H, Tang Z. Osteopontin promotes the progression of gastric cancer through the NF-kappaB pathway regulated by the MAPK and PI3K. Int J Oncol. 2014;45(1):282–90.
20. Dai J, Peng L, Fan K, Wang H, Wei R, Ji G, Cai J, Lu B, Li B, Zhang D, et al. Osteopontin induces angiogenesis through activation of PI3K/AKT and ERK1/2 in endothelial cells. Oncogene. 2009;28(38):3412–22.
21. Scheitz CJ, Tumbar T. New insights into the role of Runx1 in epithelial stem cell biology and pathology. Journal of cellular biochemistry. 2013;114(5):985–93.
22. Chimge NO, Frenkel B. The RUNX family in breast cancer: relationships with estrogen signaling. Oncogene. 2013;32(17):2121–30.
23. Hong D, Fritz AJ, Finstad KH, Fitzgerald MP, Weinheimer A, Viens AL, Ramsey J, Stein JL, Lian JB, Stein GS. Suppression of Breast Cancer Stem Cells and Tumor Growth by the RUNX1 Transcription Factor. Molecular cancer research: MCR. 2018;16(12):1952–64.
24. Chimge NO, Little GH, Baniwal SK, Adisetiyo H, Xie Y, Zhang T, O'Laughlin A, Liu ZY, Ulrich P, Martin A, et al. RUNX1 prevents oestrogen-mediated AXIN1 suppression and beta-catenin activation in ER-positive breast cancer. Nature communications. 2016;7:10751.
25. Mitsuda Y, Morita K, Kashiwazaki G, Taniguchi J, Bando T, Obara M, Hirata M, Kataoka TR, Muto M, Kaneda Y, et al. RUNX1 positively regulates the ErbB2/HER2 signaling pathway through modulating SOS1 expression in gastric cancer cells. Scientific reports. 2018;8(1):6423.
26. Liu G, Xiang T, Wu QF, Wang WX. Long Noncoding RNA H19-Derived miR-675 Enhances Proliferation and Invasion via RUNX1 in Gastric Cancer Cells. Oncology research. 2016;23(3):99–107.
27. Lu JG, Li Y, Li L, Kan X. Overexpression of osteopontin and integrin alphav in laryngeal and hypopharyngeal carcinomas associated with differentiation and metastasis. J Cancer Res Clin Oncol. 2011;137(11):1613–8.
28. Li Y, Li L, Wang JT, Kan X, Lu JG. Elevated content of osteopontin in plasma and tumor tissues of patients with laryngeal and hypopharyngeal carcinoma associated with metastasis and prognosis.

Med Oncol (Northwood Lond Engl). 2012;29(3):1429–34.
29. Luo SD, Chen YJ, Liu CT, Rau KM, Chen YC, Tsai HT, Chen CH, Chiu TJ. Osteopontin Involves Cisplatin Resistance and Poor Prognosis in Oral Squamous Cell Carcinoma. BioMed research international. 2015;2015:508587.
30. Li Q, Lai Q, He C, Fang Y, Yan Q, Zhang Y, Wang X, Gu C, Wang Y, Ye L, et al. RUNX1 promotes tumour metastasis by activating the Wnt/beta-catenin signalling pathway and EMT in colorectal cancer. Journal of experimental clinical cancer research: CR. 2019;38(1):334.
31. Xiao Y, Zhang H, Ma Q, Huang R, Lu J, Liang X, Liu X, Zhang Z, Yu L, Pang J, et al. YAP1-mediated pancreatic stellate cell activation inhibits pancreatic cancer cell proliferation. Cancer letters. 2019;462:51–60.
32. Lakshmanachetty S, Balaiya V, High WA, Koster MI. Loss of TP63 Promotes the Metastasis of Head and Neck Squamous Cell Carcinoma by Activating MAPK and STAT3 Signaling. Molecular cancer research: MCR. 2019;17(6):1279–93.
33. Sangpairoj K, Vivithanaporn P, Apisawetakan S, Chongthammakun S, Sobhon P, Chaithirayanon K. RUNX1 Regulates Migration, Invasion, and Angiogenesis via p38 MAPK Pathway in Human Glioblastoma. Cell Mol Neurobiol. 2017;37(7):1243–55.

Figures

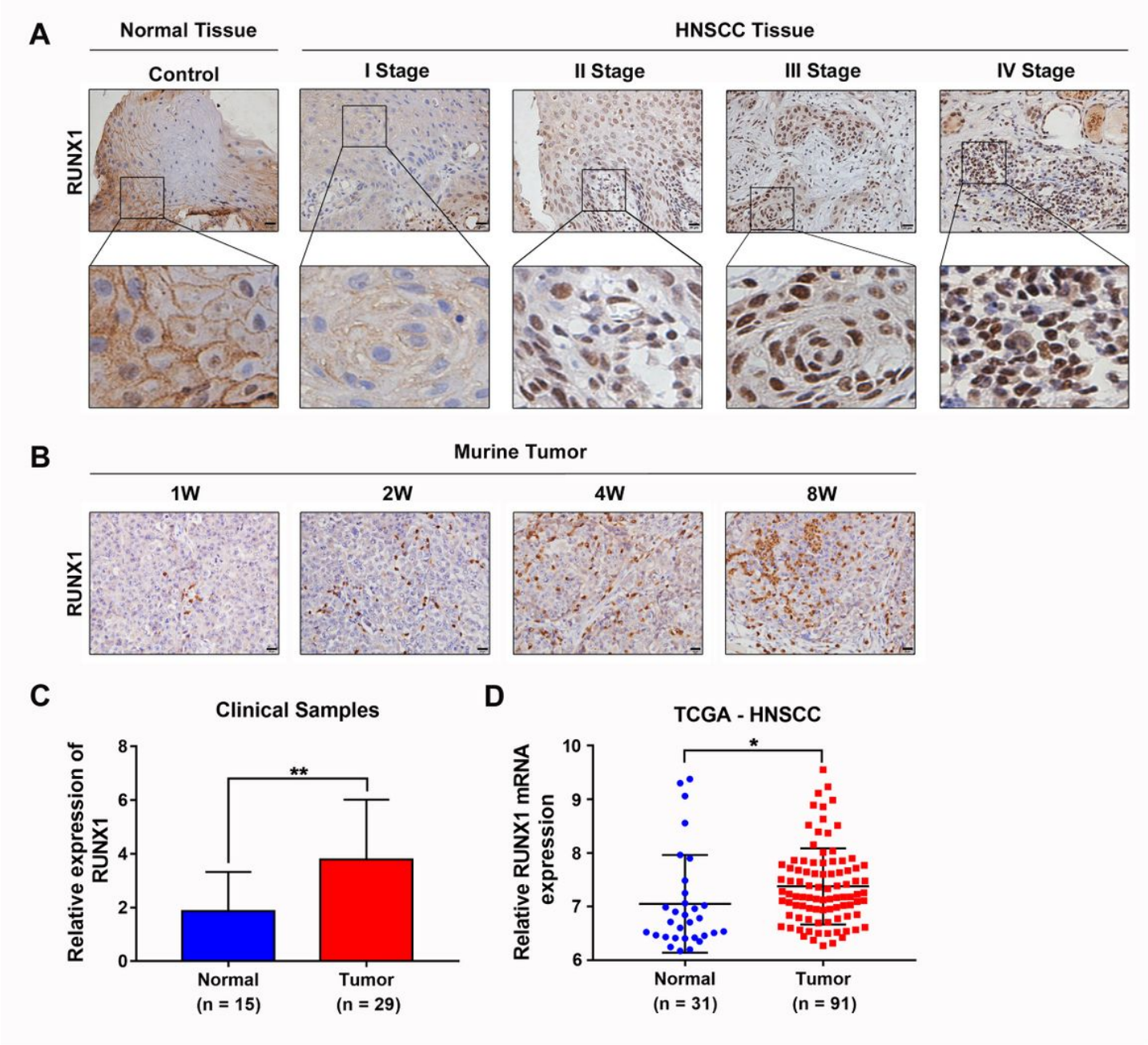

Figure 1

RUNX1 expression during cancer progression in HNSCC. (A) Representative images ofRUNX1 immunohistochemical staining between normal tissuesand HNSCC tissues (scale bar 20μm).Insets (bottom) are lower magnification (15×) images of respective cores to show a more globalview of individual samples. (B) RUNX1 staining in xenograft tumor tissues at multiple time points (1, 2, 4and 8 weeks) representing disease progression (scale bar 20μm). (C) The RUNX1 expressionscores in non-tumoral laryngeal tissues(normal) and HNSCC tissues (tumor), which contains 15 normal samples and 29 tumor samples. (D) The RUNX1 mRNA expression in tumor versus normal tissues from the TCGA database, which contains 31 normal samples and 91 HNSCC samples.*P<0.05, **P<0.01.

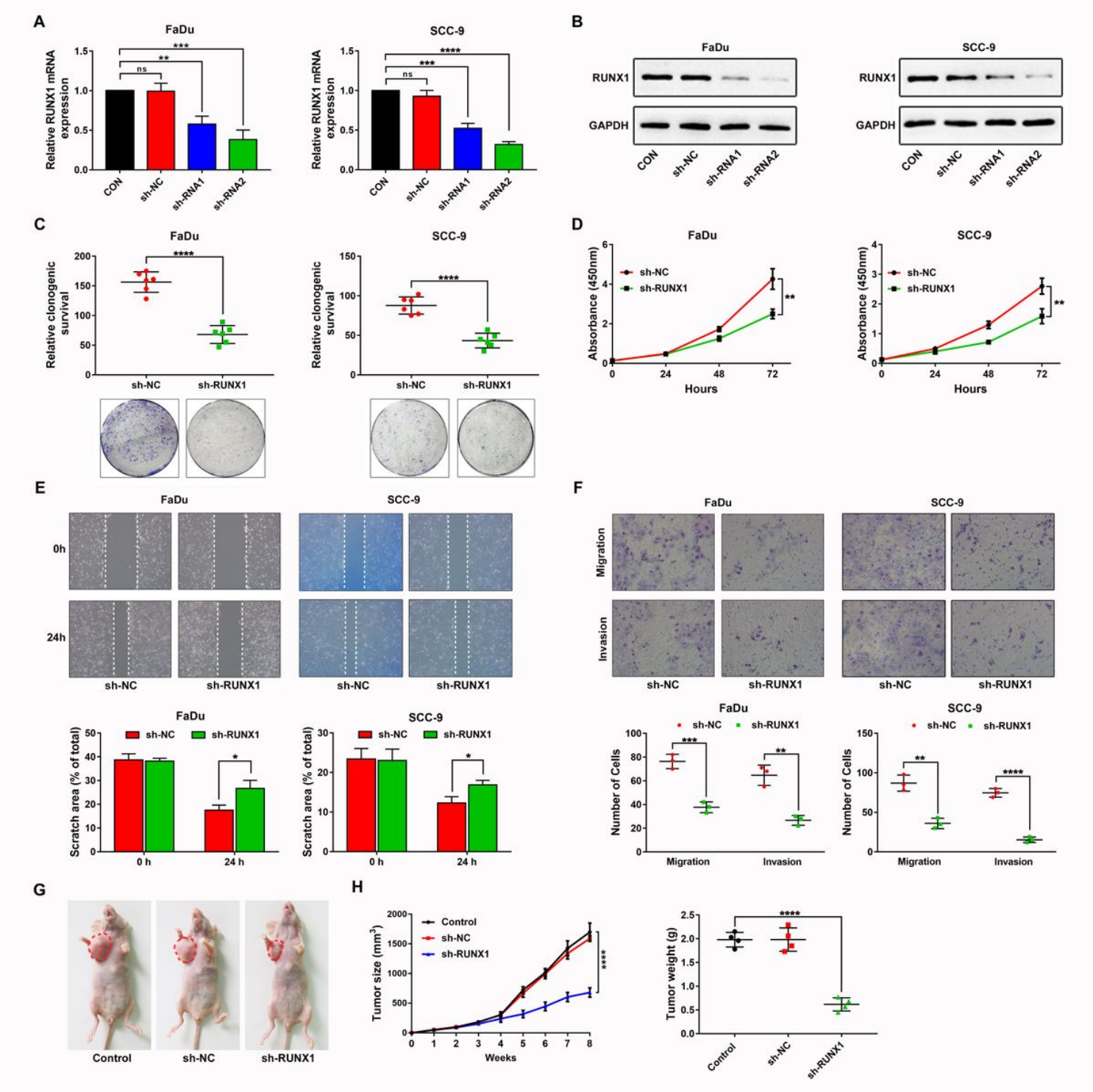

Figure 2

RUNX1 affects the progression and metastasis of HNSCC. (A) Levels of RUNX1 mRNA in the FaDu and SCC-9 cells transfected with lentiviral vector encoding shRUNX1or scrambled control were determined by real-time RT-PCR. (B) Immunoblotting analysis of RUNX1 expression in FaDu and SCC-9 cells transfectedas above. (C) Colony formation assay of FaDu and SCC-9 cellstransfectedas above. Quantitative and statistical analysis of the data (upper).The representative images of colony formation assay are presented (bottom). (D) Cell proliferation assays ofFaDu and SCC-9 cellstransfectedas above

at different time points (0h, 24h, 48h, 72h). (E) The migration ability of FaDu and SCC-9 cellstransfectedas above were assessed by wound-healing assay. Representativeimages were obtained at 0h and 24h (upper, magnification 40×) and quantified (bottom). (F) The migration and invasion ability detected by transwell assays. Representative images of FaDu and SCC-9 cells from migration and invasion assays experimentwere obtained at 24h (upper, magnification 12×) and quantified (bottom). (G) Representative images of xenograft tumor after subcutaneous injection with FaDu cells transfected with saline vehicle (Control), lentiviral empty vector (sh-NC), lentiviral vector encoding shRUNX1 (sh-RUNX1). (H) The graph of tumor growth/volumes curve at the indicated time intervals (left).Tumor weights were quantified atthe end of the experiment (right).ns, no statistical differences; *P<0.05, **P<0.01, ***P<0.001, ****P<0.0001.

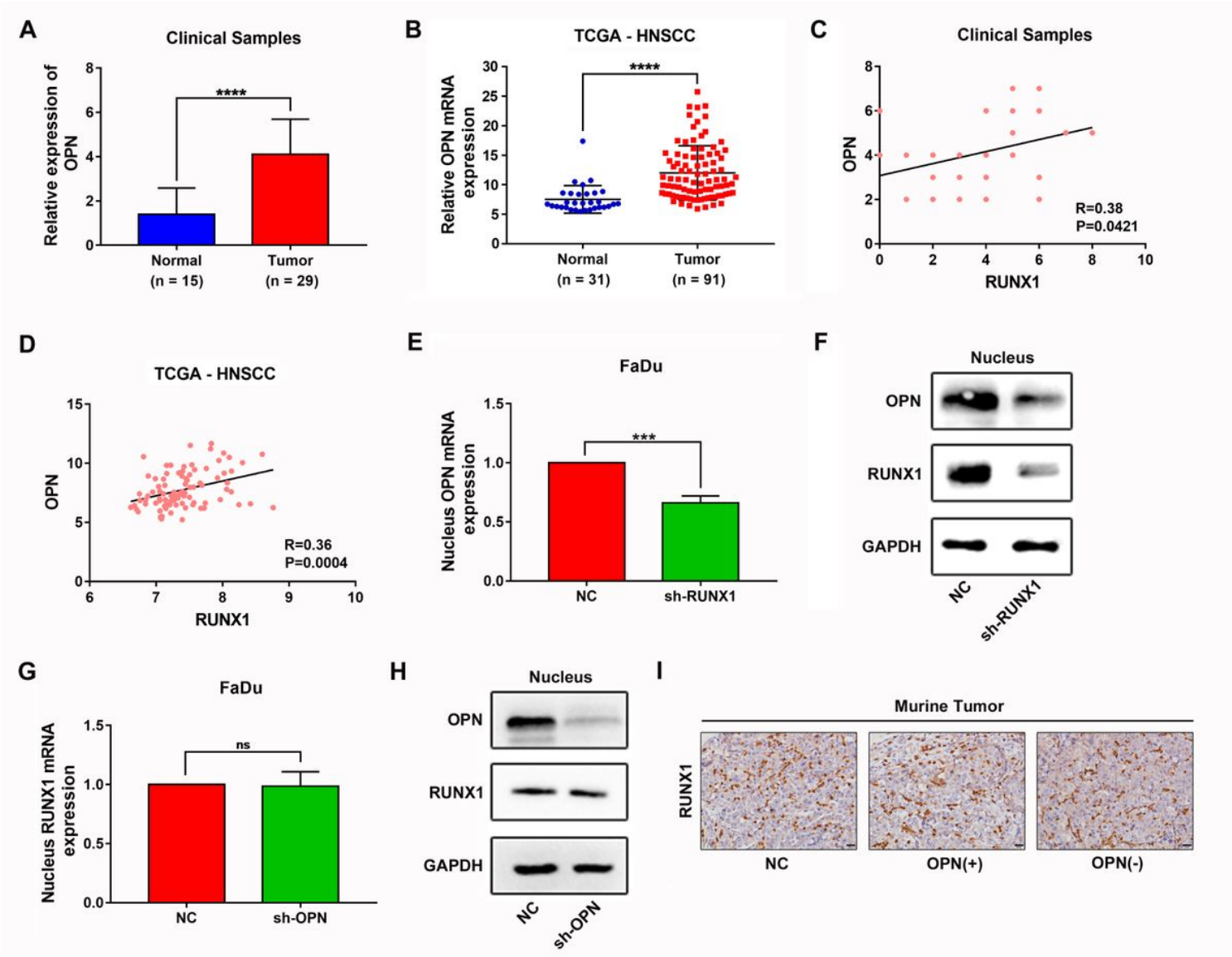

Figure 3

The interrelationship between RUNX1 and OPN in HNSCC. (A) The OPN expressionscores in non-tumoral laryngeal tissues(normal) and HNSCC tissues (tumor), which contains 15 normal samples and 29 tumor samples. (B) The OPN1 mRNA expression in tumor versus normal tissues from the TCGA database,

which contains 31 normal samples and 91 HNSCC samples. (C) Correlation analysis was performed between RUNX1 expression and OPN expression in HNSCC tissues (n = 29) and (D) in TCGAHNSCC database (n = 91). All P values are shown in the graphs.(E) Levels of nucleus OPN mRNA and (F) protein in the FaDu cells transfected with lentiviral vector encoding shRUNX1 or scrambled control were determined by real-time RT-PCR and immunoblotting analysis. (G) Levels of nucleus RUNX1 mRNA and (H) protein in the FaDu cells transfected with lentiviral vector encoding shOPN or scrambled control were determined by real-time RT-PCR and immunoblotting analysis. (I) RUNX1 staining in xenograft tumor tissues after subcutaneous injection with FaDu cells transfected with lentiviral empty vector (NC), lentiviral vector encoding OPN (OPN+), lentiviral vector encoding shOPN (OPN-) (scale bar 20μm).ns, no statistical differences; ***P<0.001, ****P<0.0001.

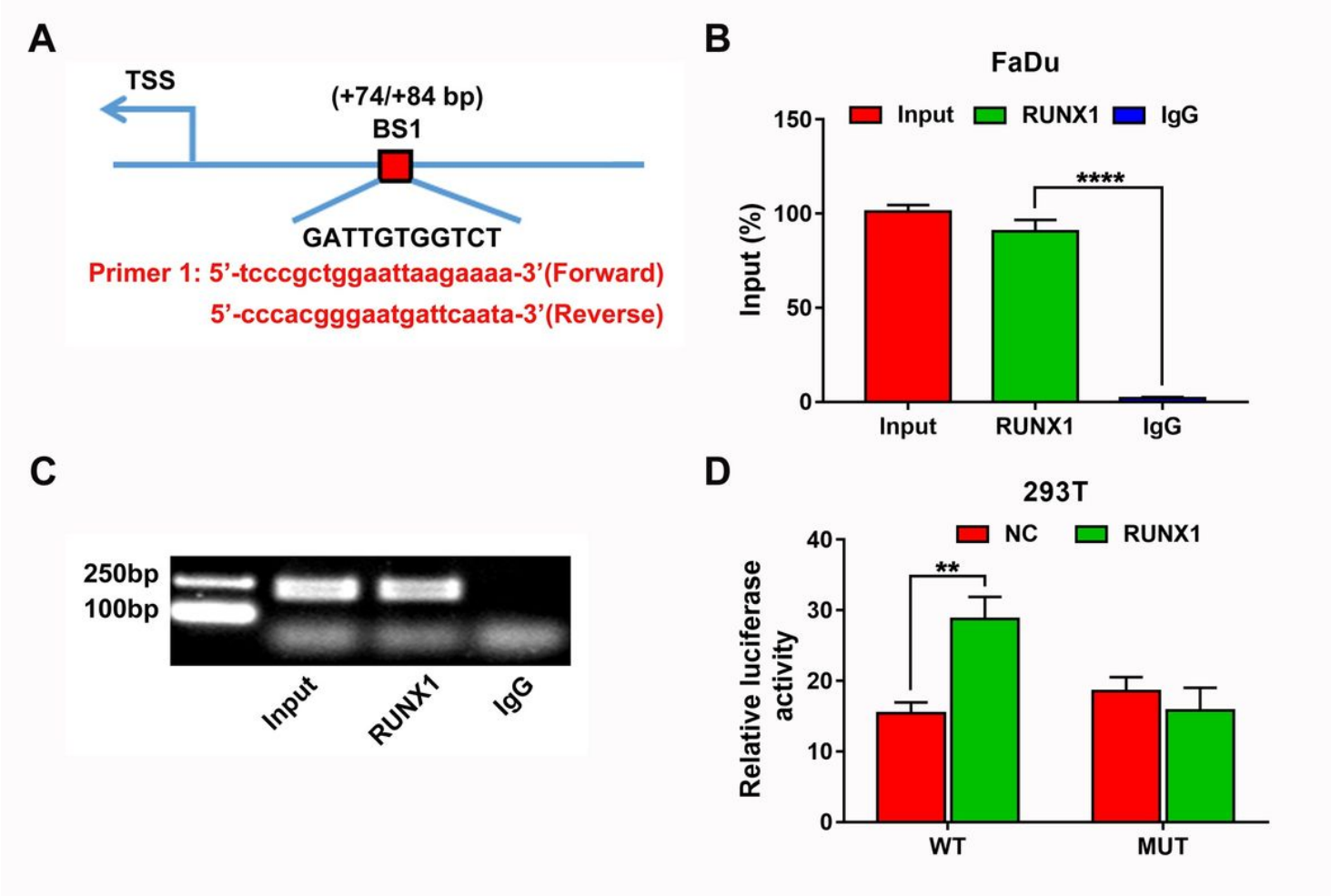

Figure 4

RUNX1 directly stimulates OPN expression at the transcriptional level (A) The predicted OPN promoter sequence bound by RUNX1 and their ChIP-PCR primers. (B-C) The binding of RUNX1 to predicted OPN promoterbinding region was confirmed in FaDu using ChIP-qPCR andChIP-PCR. IgG wasused as the control. (D) Relative OPN activitywas detected by luciferase assay in 293T cells co-transfected with RUNX1 and luciferase reporter.**P<0.01, ****P<0.0001.

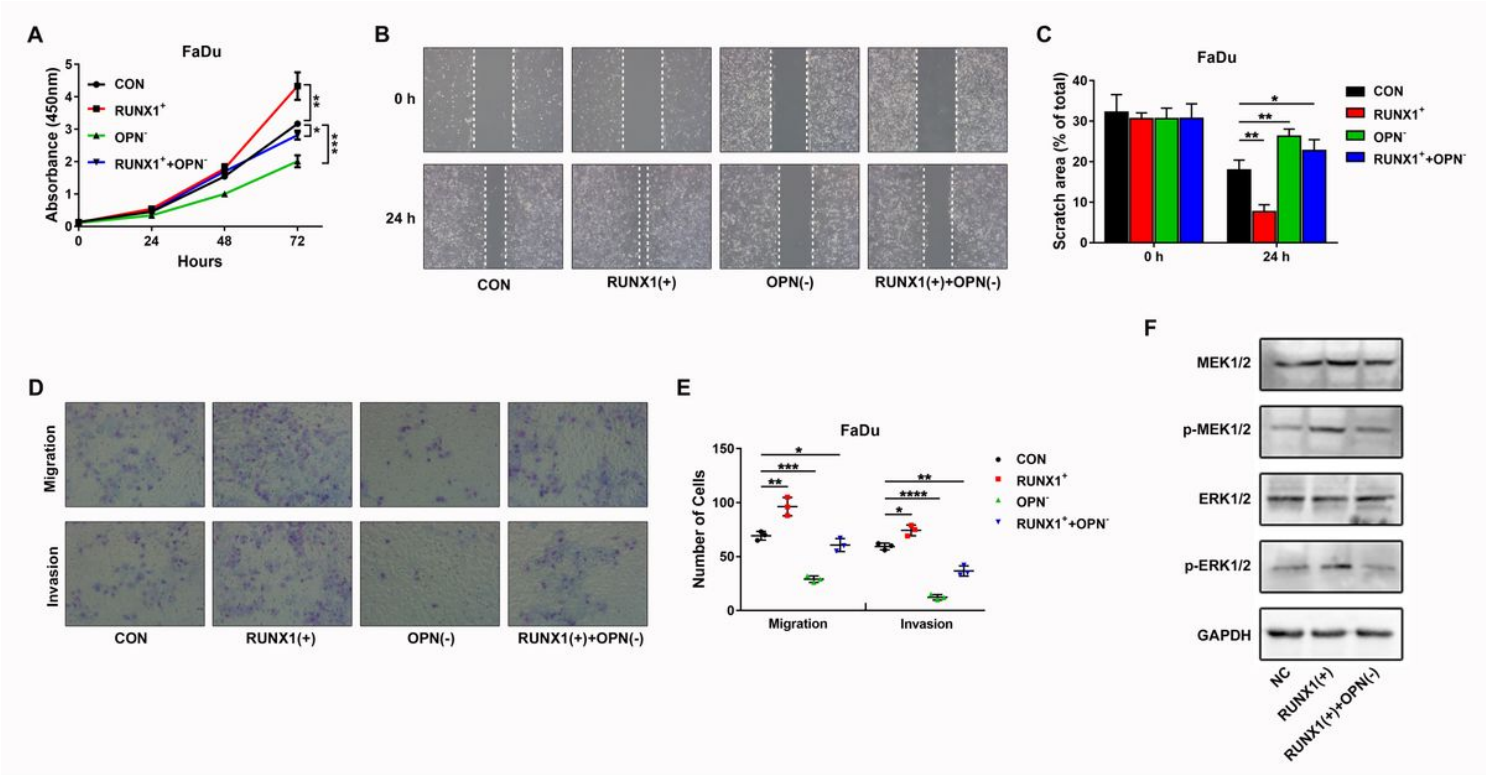

Figure 5

RUNX1 mediates HNSCC cell metastasis and MAPK pathway activation via stimulating OPN. (A) Cell proliferation assays ofFaDu cellstransfectedwith control vector (CON), lentiviral vector encoding RUNX1 (RUNX1+), lentiviral vector encoding shOPN (OPN-),or successively transfected with RUNX1+ and OPN- (RUNX1++OPN-) at different time points (0h, 24h, 48h, 72h). (B) The migration ability of FaDu cellstransfectedas abovewere assessed by wound-healing assay. Representativeimages were obtained at 0h and 24h (magnification 40×) and (C) quantitative and statistical analysis was performed. (D) The migration and invasion ability detected by transwell assays. Representative images of FaDu cells from migration and invasion assays experimentwere obtained at 24h (magnification 12×) and (E) quantitative and statistical analysis was performed. (F) Immunoblotting analysis for protein markers expression levels of the MAPK pathwayinFaDu cellstransfected as above. *P<0.05, **P<0.01, ***P<0.001, ****P<0.0001.

Supplementary Files

This is a list of supplementary files associated with this preprint. Click to download.

- Supplementalfigurelegends.docx
- Supplementalfigurelegends.docx
- FigureS5.tif
- FigureS5.tif

- FigureS2.tif
- FigureS2.tif
- FigureS3.tif
- FigureS3.tif
- FigureS1.tif
- FigureS1.tif
- FigureS4.tif
- FigureS4.tif